sustainability

MDPI

Article

Investigation on Rheological Properties and Microscopic Mechanisms of Sasobit/Buton Rock Asphalt Modified Asphalt

Wei Liu, Shaopeng Wu *, Qi Jiang, Zenggang Zhao, Xinkui Yang and Jun Xie

State Key Laboratory of Silicate Materials for Architectures, Wuhan University of Technology, Wuhan 430070, China; liuw321@whut.edu.cn (W.L.); jiang7001@whut.edu.cn (Q.J.); zhaozenggang@whut.edu.cn (Z.Z.); yangxk@whut.edu.cn (X.Y.); xiejun3970@whut.edu.cn (J.X.)
* Correspondence: wusp@whut.edu.cn

Abstract: The objective of this study is to develop a modified asphalt with excellent rheology and workability. Buton rock asphalt (BRA) composite modified warm mix asphalt (BCMWMA) was prepared, and its rheological properties and micromechanisms were investigated. Initially, warm mix asphalt (WMA) was prepared using 3 wt% Sasobit, and then four BCMWMA samples were prepared by blending 5 wt% to 20 wt% of BRA (with 5 wt% intervals). Subsequently, the microscopic morphology and modification mechanism of BCMWMA were analysed by scanning electron microscopy (SEM) and Fourier transform infrared spectroscopy (FTIR) tests. Finally, the rheological properties of BCMWMA were examined through conventional properties tests, rotational viscosity tests (RV), dynamic shear rheological tests (DSR) and bending beam rheometer tests (BBR). The results indicate that the BRA and Sasobit composite modifications primarily involve physical modification. BRA improves the high-temperature performance of the modified asphalt but reduces its low-temperature performance. Overall, the BCMWMA exhibits excellent high-temperature performance and workability, contributing to the green and sustainable development of asphalt pavement engineering.

Keywords: buton rock asphalt; Sasobit; rheological properties; workability

check for updates

Citation: Liu, W.; Wu, S.; Jiang, Q.; Zhao, Z.; Yang, X.; Xie, J. Investigation on Rheological Properties and Microscopic Mechanisms of Sasobit/Buton Rock Asphalt Modified Asphalt. *Sustainability* **2023**, *15*, 10224. https://doi.org/10.3390/su151310224

Academic Editor: Giovanni Leonardi

Received: 5 June 2023
Revised: 14 June 2023
Accepted: 21 June 2023
Published: 28 June 2023

Copyright: © 2023 by the authors. Licensee MDPI, Basel, Switzerland. This article is an open access article distributed under the terms and conditions of the Creative Commons Attribution (CC BY) license (https://creativecommons.org/licenses/by/4.0/).

1. Introduction

Roads play a vital role in modern society, connecting cities and villages and promoting economic development and social communication [1]. Asphalt binder, one of the most commonly used materials in road construction, is widely employed to create road surface layers. Asphalt possesses good plasticity and viscosity, enabling it to firmly bond aggregate particles together and form a solid pavement structure [2]. However, with the growth in road usage, asphalt pavements are subjected to various harsh environmental conditions, such as high and low temperatures, the impact of moisture and chemicals, and frequent vehicle loading [3–8]. These factors can lead to the aging, deformation, cracking and spalling of asphalt, ultimately resulting in the development of pavement distresses such as cracks, potholes and rutting [5,9,10]. These pavement issues not only cause inconvenience and safety hazards for drivers but also increase the cost of maintenance and rehabilitation while reducing the road's service life. Therefore, enhancing the performance and durability of asphalt becomes crucial for improving road quality and extending its service life.

In order to address the issues of matrix asphalt pavements, researchers have been working on enhancing the performance and durability of asphalt [11,12]. Modified asphalt serves as an effective solution widely employed in road projects. Through the addition of modifiers, the physical and chemical properties of asphalt can be adjusted to enhance its performance in terms of aging resistance, weatherability, adhesiveness and strength [13–17]. Various modifiers, including polymers, rubber and natural minerals, have been utilized in asphalt [18–21]. However, current modified asphalts still encounter certain challenges during the actual construction process.

As a natural modifier, rock asphalt (RA) plays a crucial role in asphalt modification. RA is a composite material consisting of asphalt and natural minerals, and its unique physical and chemical properties contribute to good bonding, stability and anti-aging properties [22–24]. Research has revealed that the asphalt content in RA is associated with the deposition process and typically contains 20–99.4 wt% asphalt [25], characterized by a fluffy and rough surface morphology [26]. This morphology enhances compatibility and adhesion with the matrix asphalt, as the asphalt component envelops the ash, forming numerous pore structures. The results of the four-component test have indicated that the increased asphaltene and gum components in RA modified asphalt (RAMA) enhance its performance at high temperatures [27]. These findings suggest that RA holds significant potential as a modifier in asphalt pavement, and RAMA can provide superior performance and durability. Lv et al. [28] conducted a study on the aging resistance of bio-asphalt with different doping levels of BRA, recommending an optimal doping level of 15–20 wt% BRA. Lapian et al. [29] utilized response surface methodology (RSM) to determine the optimal incorporation ratio of BRA and PET waste plastics. Ren et al. [30] conducted 60 sets of rutting tests on BRA mixtures to investigate their rutting resistance under high temperatures and the water coupling effect, establishing a Bayesian prediction model based on their findings. The model indicated that soaking time was the primary influencing factor on dynamic stability, while the amount of BRA had the least effect. Chang et al. [31] prepared BRA modified asphalt concrete using both wet and dry processes, finding that the wet process yielded better road performance. They recommended a maximum BRA additive content of 15 weight percent for the wet process and 30 weight percent for the dry process. To examine the impact of RA on the self-healing capabilities and fatigue resistance of the fine aggregate matrix, Li et al. [32] conducted fracture and fatigue healing tests, demonstrating that BRA's self-healing performance was inferior to that of Qingchuan rock asphalt. Overall, the results of these studies show the potential of rock bitumen and its modified bitumen in road materials and provide some guidance and recommendations for optimizing their road performance and durability.

To sum up, RA offers sustainability and environmental advantages compared to traditional modifiers. However, it does present certain challenges in terms of workability, the mixing temperature of SBS modified asphalt with 25% added lake asphalt is up to 200 °C. [33]. The high construction temperature of RA requires a significant amount of energy for heating and mixing the asphalt mixture. Moreover, the high construction temperatures contribute to substantial harmful emissions, which can have adverse environmental impacts [34]. Additionally, RA has relatively poor workability, and its high viscosity can lead to difficulties in mixing and compaction, thereby, affecting the construction quality and efficiency [25].

In order to address these issues in the asphalt modification process, WMA technology was developed. According to studies, WMA has become a prominent area of research in recent years due to its advantages in terms of economy, environment, and workability. WMA technology can be categorized into three classes based on its production process: foaming technology, chemical additives, and organic additives [35,36]. Sasobit, an organic wax-based warm mix agent, is known for reducing the viscosity and bonding temperature of asphalt binders, allowing for a reduction in mixing and compaction temperatures by 20 °C to 40 °C [37]. Chen et al. [38] investigated the impact of Sasobit on the rheological and physical characteristics of high-viscosity modified asphalt and found that Sasobit decreased the construction temperature of it. Liu et al. [39] examined how Sasobit influenced construction workability. Xu et al. [40] employed Sasobit and non-edible oil as viscosity-reducing additives to enhance the construction workability of rubber asphalt mixes while studying the acoustic performance of porous rubber asphalt mixes. Ramesh et al. [41] developed a new WMA mixture using 70 wt% reclaimed asphalt pavement (RAP) aggregate and determined that the optimal admixture of Sasobit, acting as a viscosity modifier, was 3 wt%. Abdollahi et al. [42] reported that Sasobit increased the workability of crumb rubber (CR) modified asphalt, and the combination of 1.5 wt% Sasobit, 15 wt% CR, and 30 wt% RAP

exhibited the best overall performance. In the study conducted by Luo et al. [43], 4% Sasobit warm mix by weight of asphalt was used to enhance workability in poured asphalt mix design. Sobhi et al. [44] employed 3 wt% Sasobit in combination with different doses of Gilsonite and found that the compound modifier reduced mixing and compaction temperatures while mitigating the negative effects of moisture sensitivity caused by Sasobit alone. To summarize, the results of these studies show the potential of Sasobit in modified asphalt to reduce construction temperatures, improve workability, and improve mix properties. These studies provide useful information and recommendations for the use of Sasobit as an additive to improve the performance and process of asphalt mixes.

Given the insufficient research on the composite modified asphalt of Sasobit and BRA, this study aims to thoroughly investigate the rheological properties and micromechanisms of this composite modified asphalt. A systematic examination of its rheological properties will enable the evaluation of its potential in enhancing the serviceability of matrix asphalt and provide a comprehensive understanding of the interaction mechanisms between the different additives. The objective of this study is to develop a modified asphalt with outstanding rheological properties and workability, offering novel solutions for road construction and improving pavement quality and sustainability. A well-planned research roadmap as shown in Figure 1 was followed.

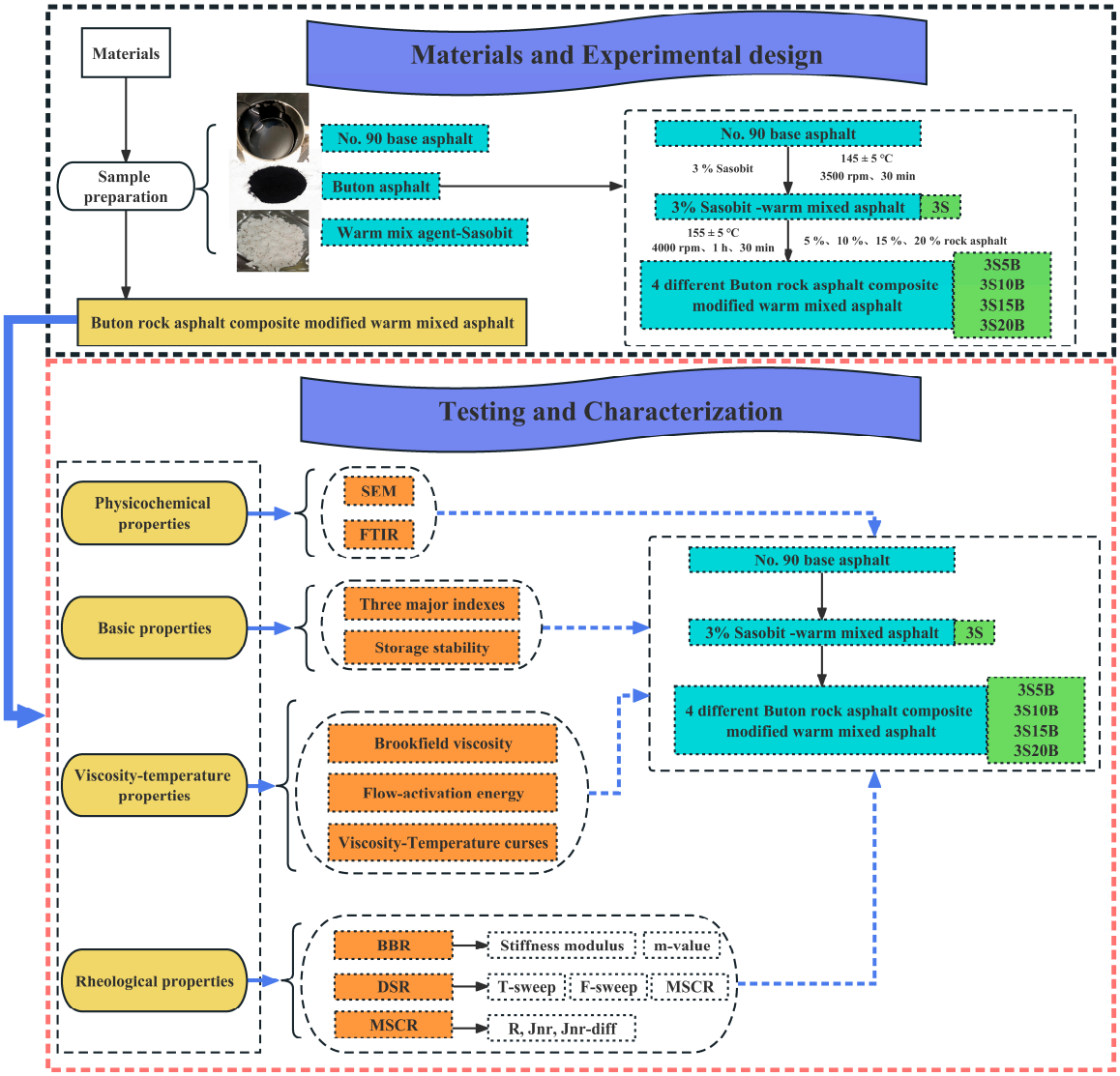


Figure 1. Research Roadmap.

2. Materials and Methods

2.1. Materials

The base asphalt utilized in this investigation was A-grade 90 road petroleum asphalt made by Panjin North Asphalt Fuel Co., Ltd., Liaoning, China. Table 1 provides a list of its physical attributes. Sasobit was provided by Henan Lu Peng Transportation Technology Co., Ltd., Zhengzhou, China, whose physical characteristics are presented in Table 2. BRA was sourced from Indonesia and provided by Hubei Zhengkang Technology and Innovation Co., Wuhan, China. According to AASHTO T315-09, the maximum size of solid modifier particles is required to be 0.25 mm. To ensure better and more uniform dispersion of the BRA in the asphalt, it was sieved through a standard sieve of 0.15 mm. The results of the BRA property tests are shown in Table 3. The chemical composition of BRA was analyzed using an X-ray fluorescence spectrometer (XRF, model Axios, Malvern Panako, The Netherlands) and the results are presented in Table 4.

Table 1. Basic properties of No. 90 asphalt.

Asphalt Properties	JTG E20-2011	Test Results	Specification Limits
Penetration at 25 °C (0.1 mm)	T0604-2011	93	80–90
Ductility at 15 °C (5 cm/min, cm)	T0605-2011	166.8	≥100
Softenting point (°C)	T0606-2011	44.7/48.13	≥42
Mass loss (%)	T0610	0.5	≤±0.8
Residual penetration ratio (%)	T0604	62	≥57
Residual ductility (%)	T0605	29	≥8

Table 2. Basic performance of Sasobit.

Sasobit Properties	Test Results
Appearance	Milky white particles
Chemical composition	Long-chain aliphatic alkanes
Density at 25 °C (g/cm^3)	0.96
Melting point (°C)	115
Flash point (°C)	290
Solubility	Water immiscible

Table 3. BRA performance indicators.

BRA Properties	Specification Limits	Test Results
Asphalt content (%)	≥20	30.5
Ash (%)	≤80	69.3
Water content (%)	≤2	0.76
Solubility of TCE (%)	≥18	28.53
Density (g/cm^3)	≤1.9	1.76
Flash point (°C)	≥230	314
Heat loss (%)	≤2	0.23
Appearance	Brown powder	Brown powder

Table 4. Chemical composition of BRA samples.

Ingredient	MgO	Al_2O_3	SiO_2	P_2O_5	SO_3	K_2O	CaO	TiO_2	MnO	Fe_2O_3	SrO	ZrO_2
Percent	1.199	2.268	8.317	0.068	4.179	0.379	33.391	0.328	0.207	6.488	0.221	0.048

2.2. Preparation of BCMWMA

To prepare the WMA, the substrate bitumen was first heated to 145 ± 5 °C to restore its fluidity. Next, Sasobit was added to the matrix asphalt in three parts at 3 wt% [45], which was produced via high-speed shearing at 3500 rpm for 30 min.

Prior research has demonstrated that the wet modification of BRA has a better effect than the dry method [31,46], and the recommended dosage generally does not exceed 20 wt% [28,32]. Based on this, the wet process for the preparation of BCMWMA was used and controlled the BRA admixture within 20 wt%. The dried BRA was then added to the WMA at 5 wt%, 10 wt%, 15 wt%, and 20 wt% at 155 ± 5 °C and sheared at 4000 rpm for 1 h to obtain BCMWMA.

To label the specimens, the substrate asphalt was referred to as "Base asphalt", the WMA as "3S", and the BRA modified warm mix asphalt as "3S5B", "3S10B", "3S15B", and "3S20B", according to the amount of rock asphalt added.

2.3. Methods

2.3.1. Fourier Transform Infrared Spectroscopy

Thermo Fisher Scientific, Waltham, MA, USA, Nicolet 6700 FTIR was used to examine the test specimens' altered chemical structure. The sampled sweep ranged between 4000 cm^{-1} and 400 cm^{-1}, with a sweep period of 64 times and a sweep precision set at 4 cm^{-1}.

2.3.2. Scanning Electron Microscope

The surface morphological characteristics of the modified asphalt were observed using a JSM-7500 cold-field emission scanning electron microscope (JEOL, Tokyo, Japan). The samples were obtained through the thermal agitation of the modified bitumen to a fluid condition and then dropping it onto clean tin foil. The tin foil with BCMWMA was subsequently warmed in an incubator for 2 h at 60 °C to promote the uniform spreading of the samples on the tin foil and remove moisture.

2.3.3. Conventional Properties Test

Three major indicators were used to test the BCMWMA: needle penetration (25 °C) (ASTM D5) [47], softening point (ASTM D36) [48], and ductility (15 °C) (ASTM D113) [49]. The softening point, needle penetration and ductility tests were repeated three times.

2.3.4. Rotational Viscosity Test

Rotational viscosity test was run with a Brookfield viscometer (DV2T, Brookfield, Massachusetts, USA) (ASTM D 4402) [50]. Using Rotor No. 27 and controlling the torque percentage between 10% and 90%, the viscosity values of the BCMWMA were tested at temperatures between 105 °C and 175 °C. The test was repeated twice for each sample.

2.3.5. Storage Stability Test

The phase separation of samples was evaluated using the softening point difference method (ASTM D7173-14) [51]. To prepare the samples, the BCMWMA was sieved through a 0.3 mm sieve, heated to a flowing state, slightly stirred, and injected into a vertical aluminum tube weighing approximately 50 g. The tubes were then placed vertically at 163 ± 5 °C over 48 h. Afterwards, the tube was kept vertical at −18 °C for not less than 4 h. After that, the top and bottom one-third portions of each sample were taken for the softening point test and the difference value was calculated. The test was repeated twice for each sample.

2.3.6. Rheological Performance Test

The dynamic shear rheometer (DSR, MCR-101, Anton Paar, Graz, Austria) was uesd to evaluate the rheological characteristics of asphalt specimens at moderate to high temperatures. The strain controlled mode was used as the loading mode and the test conditions are presented in Table 5. The low-temperature rheological characteristics were evaluated using the BBR test. Each test was repeated twice for each sample.

Table 5. Dynamic rheological performance test conditions of BRA modified warm mix asphalt.

Test Items	Temperature Range	Loaded Strain/Stress	Rotor Diameter	Parallel Plate Clearance
High temperature scan test	30~80 °C	12%	25 mm	1 mm ± 0.05 mm
Medium temperature scan test	−10~30 °C	0.5%	8 mm	2 mm ± 0.05 mm
Frequency scan test	46 °C, 52 °C, 58 °C, 64 °C, 70 °C	0.5%	25 mm	1 mm ± 0.05 mm
MSCR test	58 °C	0.1 kPa/3.2 kPa	25 mm	1 mm ± 0.05 mm

2.3.7. Multi-Stress Creep Recovery (MSCR) Test

The resistance of BCMWMA to high temperature deformation was determined using MSCR according to ASTM D7405-10A [52]. The test conditions are shown in Table 5. The test consisted of a 30-cycle creep and recovery process, with the initial ten cycles occurring during a 0.1 kPa loading phase to accommodate the sample. The test was repeated twice for each sample.

A section of the strain response of 3S15B to 0.1 kPa stress at 58 °C is shown in Figure 2. And the creep recovery rate for a single cycle was determined using Equations (1) and (2). The amount of non-recoverable creep flexibility J_{nr} was calculated based on Equations (3)–(6) for differing stress grades (0.1 and 3.2 kPa), as well as the average scores of R and J_{nr}. Additionally, Equation (7) was utilized to determine the stress sensitivity index $J_{nr-diff}$.

$$J_{nr}(\sigma, N) = \frac{\varepsilon_r - \varepsilon_0}{\sigma} \tag{1}$$

$$R(\sigma, N) = \frac{\varepsilon_c - \varepsilon_r}{\varepsilon_c - \varepsilon_0} \times 100 \tag{2}$$

$$J_{nr0.1} = \frac{\sum_{N=11}^{20} J_{nr}(0.1, N)}{10} \tag{3}$$

$$R_{0.1} = \frac{\sum_{N=11}^{20} R(0.1, N)}{10} \tag{4}$$

$$J_{nr3.2} = \frac{\sum_{N=11}^{20} J_{nr}(3.2, N)}{10} \tag{5}$$

$$R_{3.2} = \frac{\sum_{N=11}^{20} R(3.2, N)}{10} \tag{6}$$

$$J_{nr-diff} = \frac{J_{nr3.2} - J_{nr0.1}}{J_{nr0.1}} \times 100 \tag{7}$$

where: ε_0 is the shear strain at the beginning of the creep. ε_c is the shear strain at the end of creep. ε_r is the shear at the end of the recovery phase. σ is the stress applied by the test, kPa. N refers to the amount of cycles of creep recovery, J_{nr} is the amount of non-recoverable creep flexibility, kPa^{-1}, and R is the creep recovery rate, %. $J_{nr-diff}$ is the stress sensitivity index.

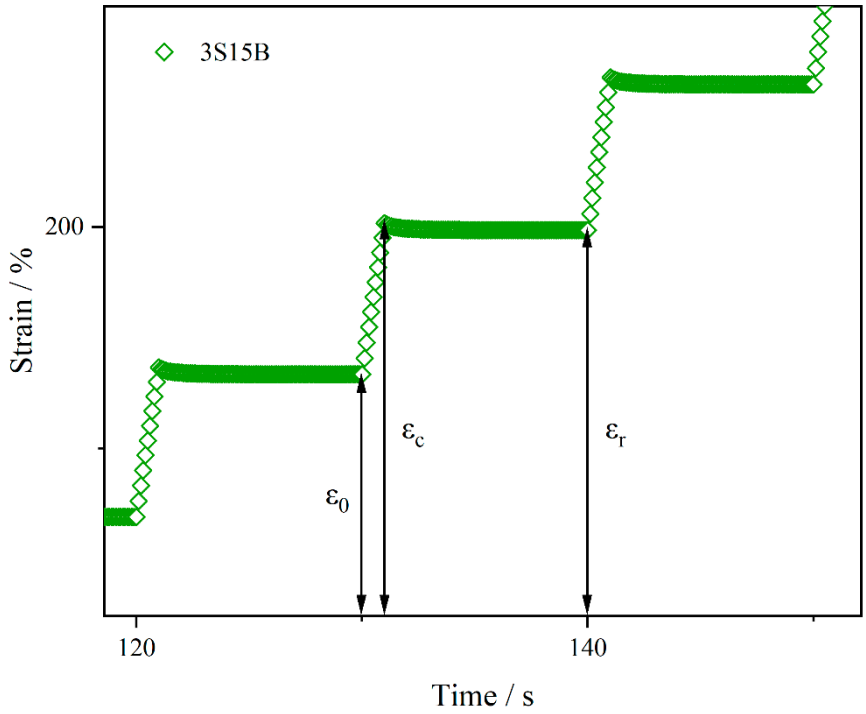


Figure 2. Strain response of a 3S15B binder measured at 0.1 kPa, 58 °C (*N* = 13, 14, 15).

2.3.8. Bending Beam Rheometer (BBR) Test

The BBR test was conducted at −6 °C to −24 °C (interval 6 °C). And according to ASTM D 6648 [53], when loaded for 60 s, the creep rate should be above 0.3 and the creep rigidity should be below 300 MPa. The test was repeated three times for each sample.

3. Results and Discussions

3.1. Physicochemical Properties of BCMWMA

SEM images of the BRA modifier at different magnifications are shown in Figure 3. It can be seen that the surface morphology of the BRA is complex and full of grooves and folds. Combined with the SEM images of the test samples (as in Figure 4), it is obvious that the BRA's intricate surface morphology benefits the combination of BRA and asphalt. Figure 4a,b are the SEM images of matrix asphalt and WMA, respectively. Their surfaces are flat and smooth, and some areas show a regular texture caused by the tinfoil backing. The surface morphological characteristics of the bitumen samples after incorporation of the BRA, in ascending order of incorporation ratio, are shown in Figure 4c–f. From which it can be seen that the transition at the interface between rock asphalt and WMA is smooth; no obvious boundary is produced; and the asphalt is well wrapped with rock asphalt particles, which further suggests that the BRA and WMA are compatible. On the other hand, there were obvious bumps on the surface, which might be caused by the agglomeration of the ash component of the BRA particles. As the BRA content increased, the agglomeration phenomenon gradually intensified. The ash in 3S5B (Figure 4c) and 3S10B (Figure 4d) samples showed a small range agglomeration with overall uniform dispersion, but the ash in 3S15B (Figure 4e) sample showed a larger scope agglomeration with large bumps, and the ash in 3S20B (Figure 4f) sample showed a stronger agglomeration with two large-scale agglomerates of ash are not favorable. The extensive agglomeration of ash is not conducive to the compatibility of the three-phase system of BCMWMA and weakness the storage stability.

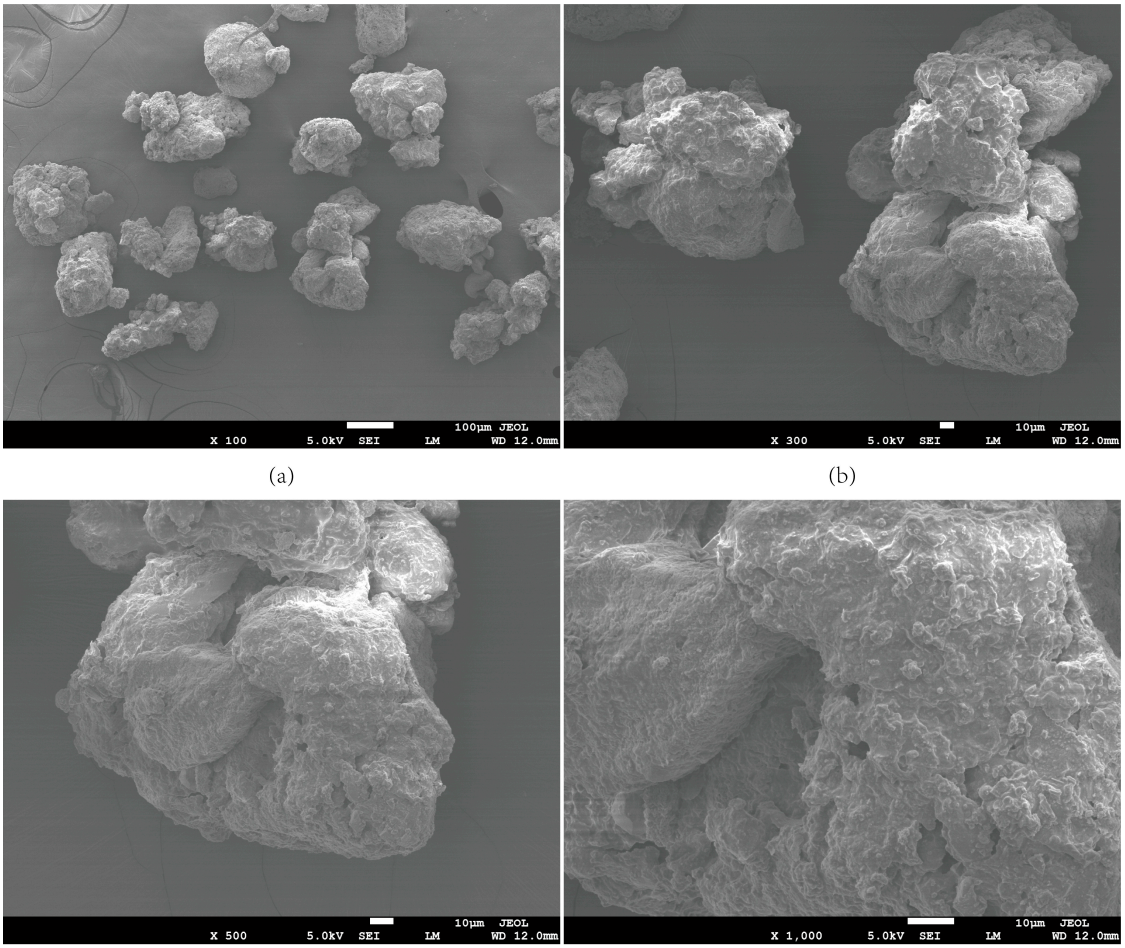


Figure 3. BRA scanning electron microscope (SEM) images: (**a**) ×100, (**b**) ×300, (**c**) ×500, (**d**) ×1000.

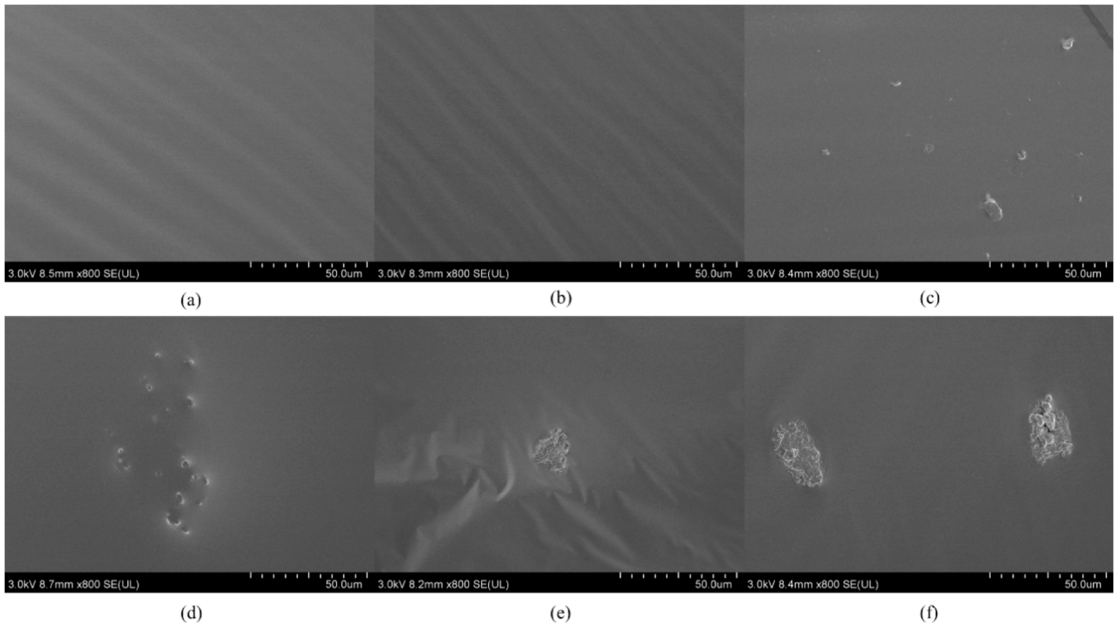


Figure 4. Scanning electron microscope images of the test specimens (×800): (**a**) Base asphalt (**b**) 3S (**c**) 3S5B (**d**) 3S10B (**e**) 3S15B (**f**) 3S20B.

Utilizing BRA and Sasobit to examine how composite alteration affects the chemical make-up of specimens, FTIR testing was performed. Figure 5 shows that the main absorption peaks of the tested samples include the sulfoxide group's stretching vibration (S=O) at 1033 cm^{-1}, the umbrella vibration of methylene (−CH2) at 1375 cm^{-1}, the shear vibration of methylene (−CH2) at 1459 cm^{-1}, the stretching vibration of the benzene ring skeleton (C=C) at 1602 cm^{-1}, the stretching vibration of the carbonyl group (C=O) in the aldehyde group at 1730 cm^{-1}, the symmetric stretching vibration of C-H in methylene at 2855 cm^{-1}, the asymmetric stretching vibration of C−H in methylene at 2925 cm^{-1} and the asymmetric stretching vibration of C−H in methylene at 2954 cm^{-1}. Notably, the spectra of the base asphalt remained unchanged after adding warm agent and BRA, and no new peaks were generated; this is consistent with the findings of the literature [54]. Therefore, it is evident that the inclusion of a warm agent and BRA primarily results in a physical co-blending process and does not significantly impact the chemical structure of the asphalt.

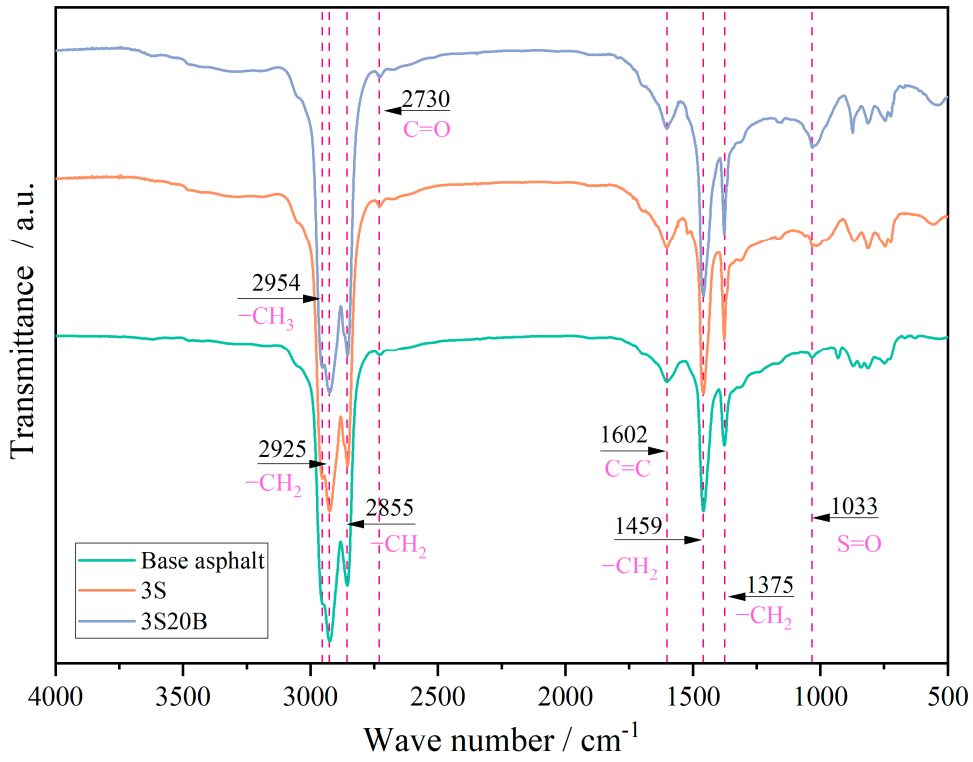


Figure 5. FTIR spectra of asphalt samples.

3.2. Basic Properties of BCMWMA

The results for the three major indexes of the BCMWMA are presented in Figure 6. From the results, as compared to raw asphalt, the utilization of a warm agent decreased the ductility by 19.8%, raised the softening point by 0.47%, and reduced the needle penetration by 3.1%. Furthermore, the ductility and needle penetration of BCMWMA gradually declined, whereas the softening point gradually raised with increasing BRA content, as compared to the warm mix asphalt [55]. For instance, when the BRA content was 5 wt%, 10 wt%, 15 wt%, and 20 wt%, the needle penetration decreased by 2.4%, 11.2%, 13.7%, and 16.6%, respectively. And the softening point increased by 1.29%, 3.02%, 5.29%, and 6.57%, respectively. However, the ductility decreased by 39.4%, 58.4%, 75.2%, and 81.3%, respectively. This suggests that the incorporation of BRA into WMA can enhance the asphalt's stiffness, reduce its low temperature anti-cracking performance and temperature sensitivity.

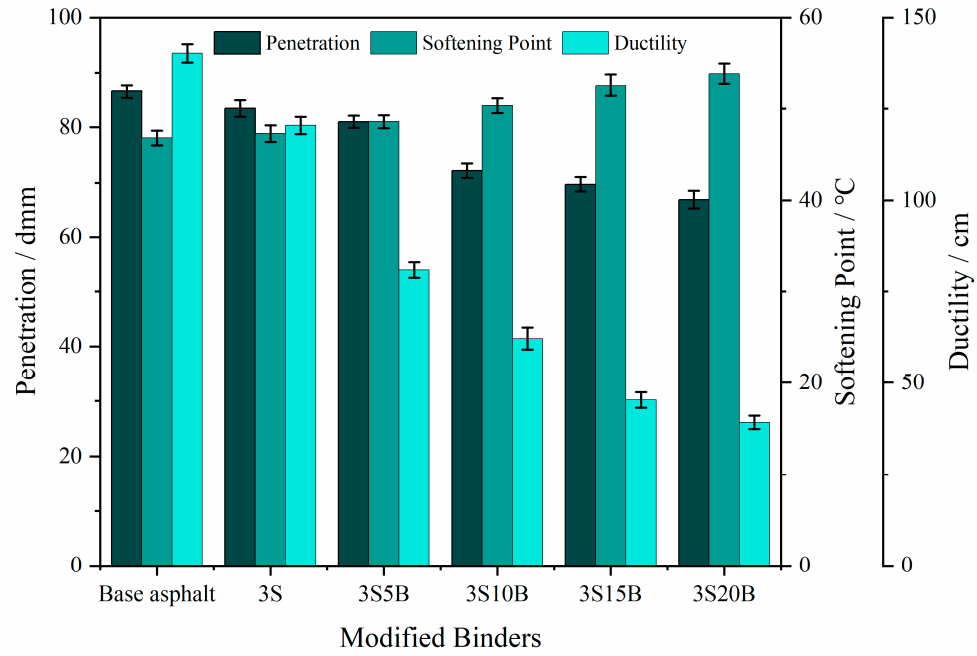


Figure 6. The three major indexes test results.

The softening point difference method was used to evaluate the storage stability of BCMWMA. Figure 7 displays the findings and errors, showing that the warm-mixed additive's impact on the difference in softening point with base asphalt was negligible, as it only increased by 0.1 °C. Furthermore, with rising BRA content, the softening point difference gradually increased. This could be due to the fact that the BRA has a density about 1.8 times that of matrix bitumen. While the complex morphology of BRA and other factors promote its compatibility with the base asphalt, a softening point difference value greater than the allowed specification value (2.5 °C) was obtained when blended with 20 wt% BRA, rendering it unsuitable for use. Therefore, the maximum amount of BRA blending obtained from the storage stability test was 15 wt%.

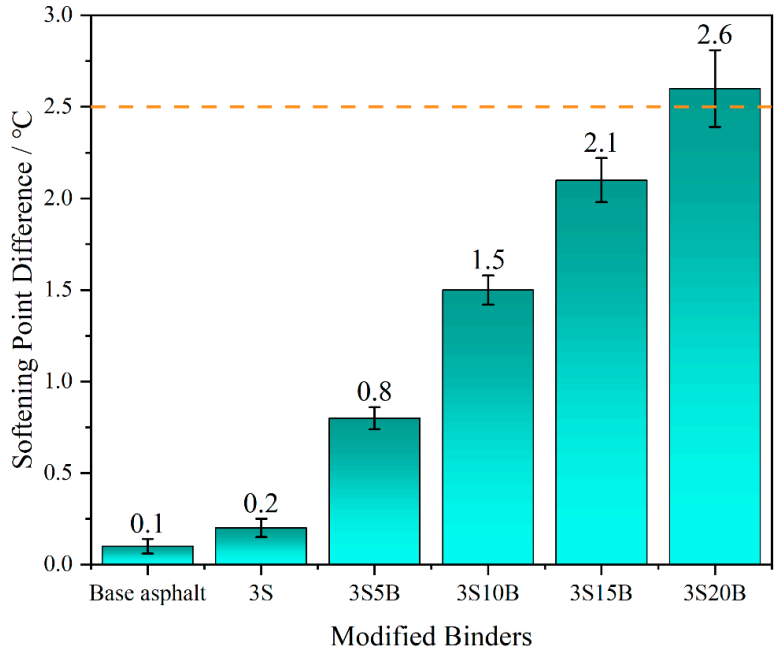


Figure 7. Softening Point Difference test results.

3.3. Viscosity-Temperature Properties of BCMWMA

3.3.1. Brookfield Viscosity

Viscosity is a crucial parameter that reflects the temperature sensitivity of asphalt samples and their construction workability. Figure 8 shows the viscosities of the matrix bitumen, WMA, and BCMWMA at eight test temperatures between 105 °C and 175 °C (with a 10 °C temperature interval). The findings demonstrate that the viscosity of the BCMWMA increases with increasing BRA admixture, indicating that the BRA has potential to enhance the elevated temperature performance of asphalt. Yet, the viscosity of the asphalt specimens tended to decrease as the temperature increased. WMA has a viscosity that is 10.5% more than base asphalt at 105 °C. When the temperature reaches 115 °C and above, WMA has a lower viscosity than base asphalt, while the viscosity value of 3S5B begins to be slightly greater than warm mix asphalt but slightly lower than base asphalt. This is due to the fact that the melting temperature of Sasobit is about 115 °C. Sasobit increases the viscosity when the temperature falls below the melting point [56]. Based on these results, the rotary viscosity values at 115 °C and above were chosen for subsequent analysis of the flow activation energy and mixing-compaction temperature of the test samples.

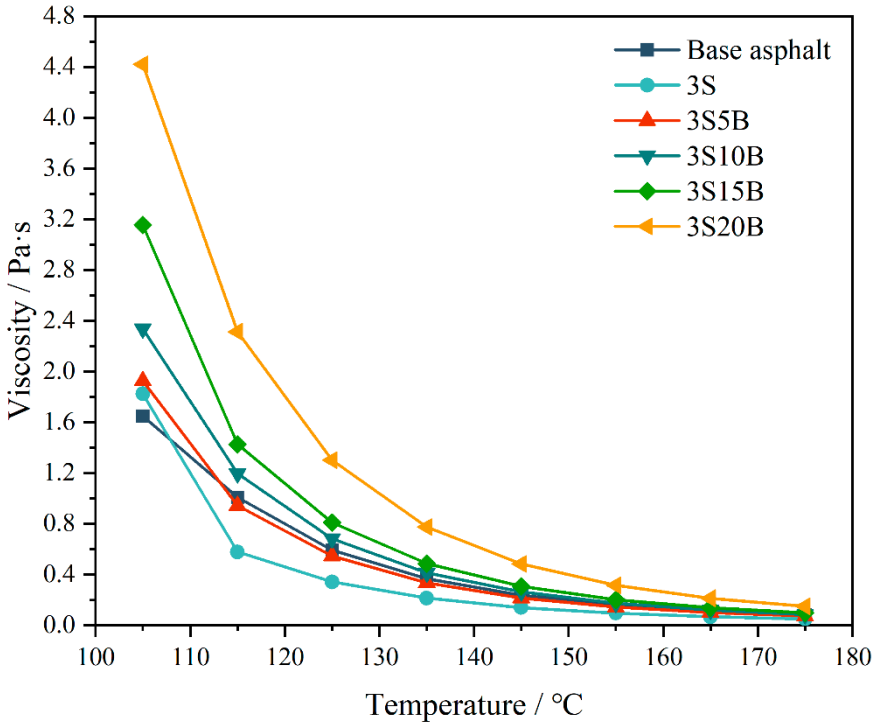


Figure 8. Viscosity-temperature curves of asphalt.

3.3.2. Flow Activation Energy

The flow activation energy (E_η) represents the energy required to overcome the action of surrounding molecules when the macromolecule leaps to the cavity. The larger the energy, the more sensitive the viscosity is to changes in temperature. Furthermore, as E_η decreases, the fluidity of the fluid becomes better. In other words, a greater E_η suggests that viscosity is more temperature-dependent. Equation (8) shows how to derive the flow activation energy from the Arrhenius equation [57].

$$\eta = A \cdot e^{E_\eta / RT} \tag{8}$$

$$\ln\eta = \ln A + \frac{E_\eta}{R} \times \frac{1}{T} \tag{9}$$

where, the viscosity of rotation (in Pa·s) is denoted by η, while T (in Kelvin) represents the temperature, and R (8.314 J/(mol·K)) represents the molar gas constant. Asphalt flow activation energy (kJ/mol) is represented by E_η and A denotes the regression coefficient.

Considering the Arrhenius equation's logarithm on both sides, we can obtain Equation (9), which is then fitted to the data (as shown in Figure 9). The resulting slope can be used to calculate E_η. Table 6 displays the fitted variables. According to the findings of the fitting, the Arrhenius equation can well characterize the link between the rheological characteristics and energy (temperature) of the BCMWMA, as evidenced by the correlation coefficient (R^2) of about 0.997. Furthermore, Sasobit reduces E_η by 2.85% relative to matrix asphalt. This means that Sasobit can lower the flow energy threshold of BCMWMA, so that the asphalt molecules in warm mix asphalt require less energy to leap to cavities and are more likely to leap, resulting in better flowability and lower viscosity on a macroscopic scale. Conversely, the E_η of BCMWMA is larger than that of WMA. This indicates that the addition of BRA raises the energy threshold for the flow behavior of warm mix asphalt, resulting in poorer flow and higher viscosity on a macroscopic scale. From the analysis of colloid theory, it appears that BRA increases the dispersion medium and reduces the dispersed phase by absorbing some lighter components while increasing the asphaltene content, which in turn leads to an increase in BCMWMA viscosity and a decrease in asphalt fluidity.

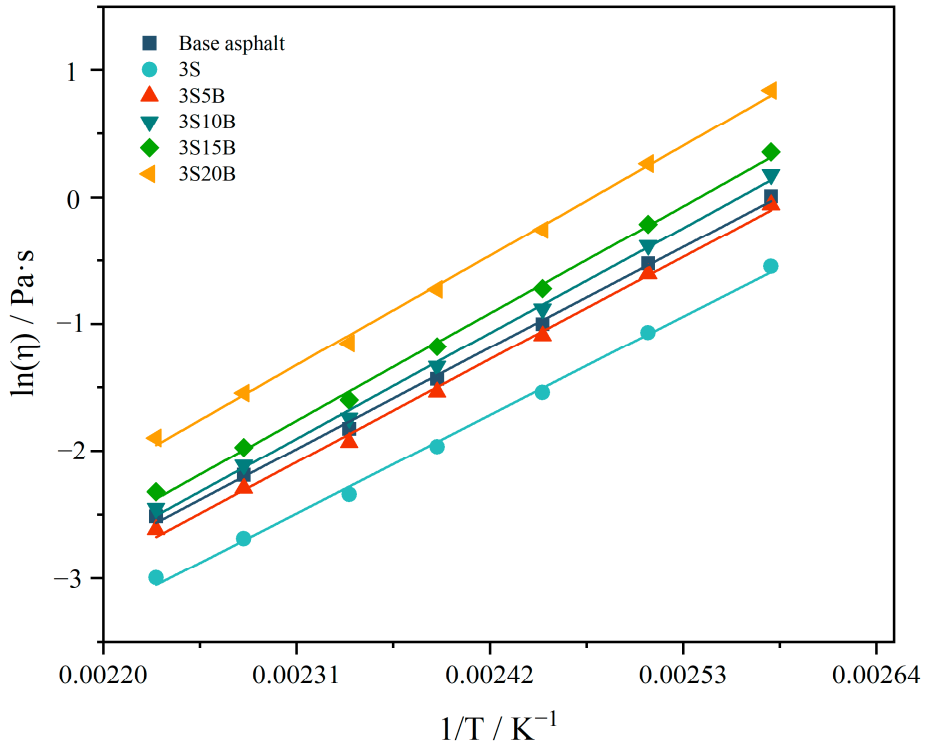


Figure 9. Fitting results of Arrhenius equation.

Table 6. Fitting parameters of Arrhenius equation.

Asphalt	Fitting Line	R^2	Slope (E_η/R)	E_η (kJ/mol)
Base asphalt	Y = 7247.31x − 18.73	0.998	7247.31	60.25
3S	Y = 7040.45x − 18.76	0.997	7040.45	58.53
3S5B	Y = 7354.69x − 19.08	0.997	7354.69	61.15
3S10B	Y = 7554.68x − 19.36	0.997	7554.68	62.81
3S15B	Y = 7689x − 19.52	0.997	7689	63.93
3S20B	Y = 7866.74x − 19.5	0.997	7866.74	65.4

3.3.3. Effect of Warm Mixing

To better compare the impact of BRA on the WMA, the manufacturing temperatures of samples were calculated in this study. This was accomplished by fitting the rotational viscosity of the measured samples using Saal's equation (shown in Equation (10)) in ASTM D2493 [58]. Figure 10 displays the fitting curves, while Table 7 displays the fitted values. Subsequently, using rotational viscosities of 0.17 ± 0.02 Pa·s for mixing and 0.28 ± 0.03 Pa·s, for compaction. Table 8 presents the outcomes.

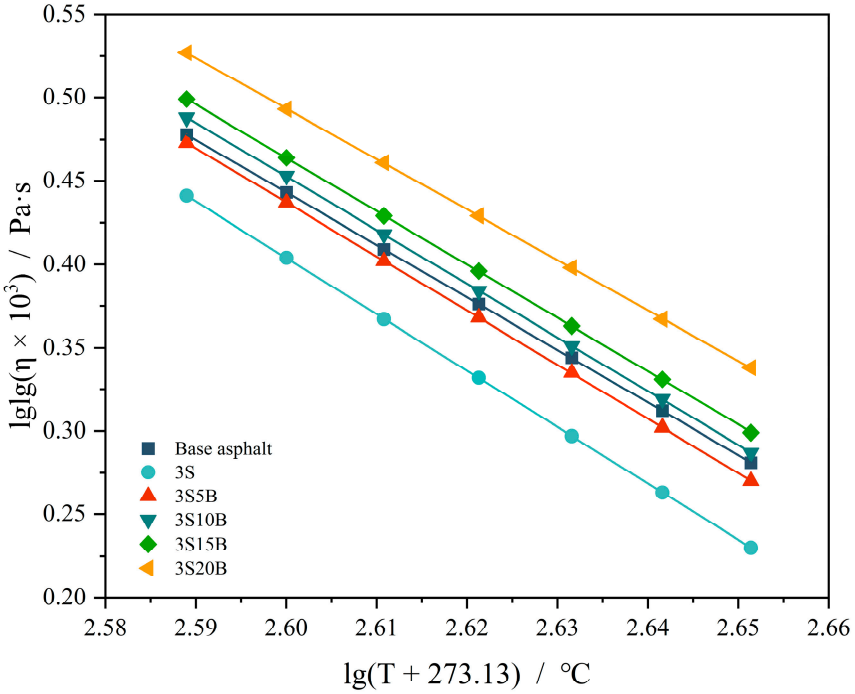


Figure 10. The fitting results of Saal's equation.

Table 7. The fitting result of viscosity temperature curves via Saal's equation.

Asphalt	Equation	Slope	R^2
Base asphalt	Y = 8.64 − 3.15x	3.15	0.986
3S	Y = 9.2 − 3.38x	3.38	0.983
3S5B	Y = 8.88 − 3.25x	3.25	0.989
3S10B	Y = 8.83 − 3.22x	3.22	0.981
3S15B	Y = 8.78 − 3.2x	3.2	0.984
3S20B	Y = 8.37 − 3.03x	3.03	0.999

Table 8. Mixing and compaction temperature of the asphalt specimens (°C).

Types	Base Asphalt	3S	3S5B	3S10B	3S15B	3S20B
Mixing temperature	150.6–156.9	137.7–143.3	148.1–154.1	153–159.1	156.6–162.8	168.3–175
Compaction temperature	138.8–143.8	127–131.5	136.6–141.5	141.3–146.3	144.8–149.8	155.5–160.9

The fitting findings demonstrate that Saal's formula accurately describes the viscosity temperature relationship, as evidenced by the high correlation coefficients (greater than 0.98) for all asphalt samples. Related literature [59,60] pointed out that the absolute slope value of the fitting formula could assess the temperature susceptibility of the test samples. As indicated in Table 7, the slope of WMA is the highest among all test temperatures, with the slope of 3S being 7.3% more than the basic asphalt's slope. This is due to the full melting of the warm agent at the test temperature and the increase of the lightweight

component. Meanwhile, the slope of BCMWMA decreased by 3.85%, 4.73%, 5.33%, and 10.36%, respectively, with an increasing BRA admixture compared to 3S, indicating that the sensitivity of WMA to temperature is greatly decreased by the BRA. This is due to the fact that the addition of BRA requires higher energy for the movement of asphalt molecules, which enhances the BCMWMA's thermal stability. This is in accordance with the softening point test's findings.

Based on the "Asphalt Mixture Modification Additives Part 5 Natural Asphalt" (JTT_860.5-2014) standard [61], an indoor test with natural asphalt modified with No. 70 or No. 90 asphalt preparation mix specifies a mixing temperature of 170–180 °C and a compaction molding temperature of 160–165 °C. All asphalt specimens in this study meet these specification requirements, with the warm mix effect decreasing as the BRA dosage increases. Specifically, the mixing temperature of the 3S sample was reduced by approximately 13 °C and the compaction temperature was reduced by about 12 °C, relative to the base asphalt. The mixing temperature of the BCMWMA was reduced by about 21.9 °C, 17 °C, 13.4 °C, and 1.7 °C with increasing blending quantity compared to the parameters stated in the specification (all taken as the lower limit of temperature), and the compaction temperature was reduced by 23.4 °C, 18.7 °C, 15.2 °C, and 4.5 °C, respectively. These findings reveal that the BCMWMA has a significant warm mix effect when the amount of BRA does not exceed 15 wt%.

$$\lg\lg(\eta(T) \times 1000) = n - m \times \lg(T + 273.13) \tag{10}$$

where, n denotes the intercept; $\eta(T)$ denotes the viscosity at T degrees Celsius, Pa·s; T is the temperature, °C; and m denotes the slope.

3.4. Rheology Properties of BCMWMA

BBR Test Results

Figures 11 and 12 display the S and m values of the different asphalt samples. The rigidity modulus of warm mix asphalt increases and the creep rate decreases compared to the base asphalt. Moreover, as the amount of BRA admixture increases, the stiffness modulus of the BCMWMA tends to increase, while the creep rate has the opposite trend, compared to warm mix asphalt. Another trend observed across all test samples is the reduction in creep rate and the rise in stiffness modulus as the test temperature decreases.

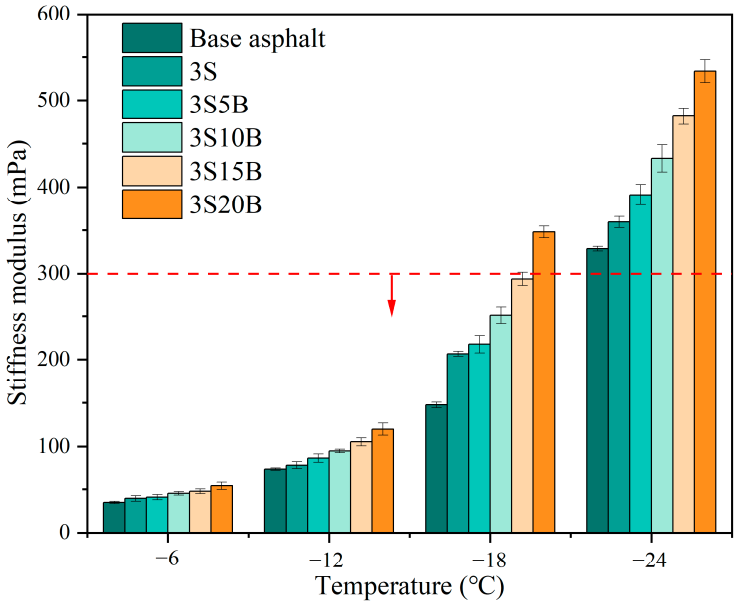


Figure 11. Stiffness modulus of asphalt samples.

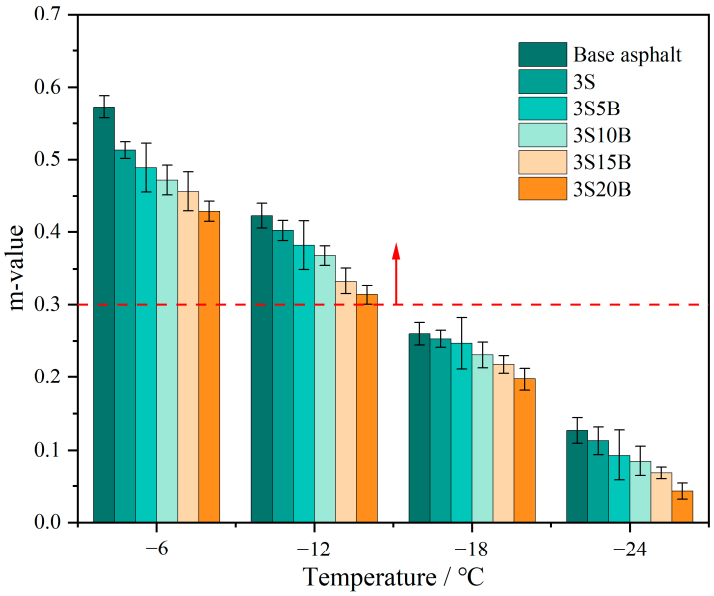


Figure 12. M-value of asphalt samples.

At temperatures of −12 °C and above, all asphalt stiffness modulus and creep rates meet the specification requirements, with stiffness modulus values below 300 MPa and creep rates greater than 0.3. However, at −18 °C, only the stiffness modulus of sample 3S20B did not meet the requirement, while all other samples had a stiffness modulus below 300 mPa, but none of them had the required m value. At −24 °C, all tested samples failed. These results indicate that BRA reduces the cold resistance of WMA and the higher the doping amount the worse the low temperature performance, which aligns with the ductility test findings. The BBR test results show that the lowest temperature at which BRA meets the requirement is −12 °C.

3.5. Temperature Sweep Test Results

Two quantitative measured values of the temperature-dependent rheological properties of asphalt are the G^* and δ, which are computed using DSR. More asphalt rigidity is indicated by a larger G^* value, and the proportion of resilience to stickiness is shown by δ, with smaller phase angles indicating a larger proportion of elastic components.

Figures 13 and 14 depict the samples' G^* and δ tested at different temperatures. The results reveal that the values indicate a tendency in the opposite direction: the samples' G^* decrease significantly with rising temperature. The addition of warm agent raises complex modulus while lowering phase angle relative to the base asphalt. Furthermore, the G^* of the BCMWMA continuously rises, while the δ steadily falls, with increasing BRA content relative to warm mix asphalt. These results imply that the Sasobit increases the deformation resistance and resilience of the matrix asphalt, while adding the BRA modifier further strengthens the deformation resistance of WMA.

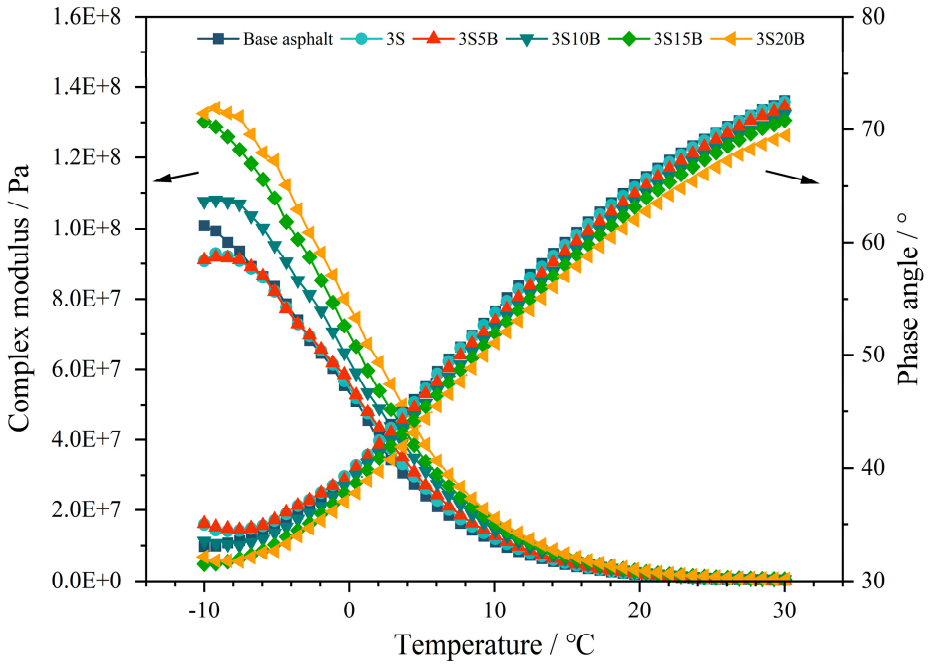


Figure 13. Temperature scan results at −10~30 °C.

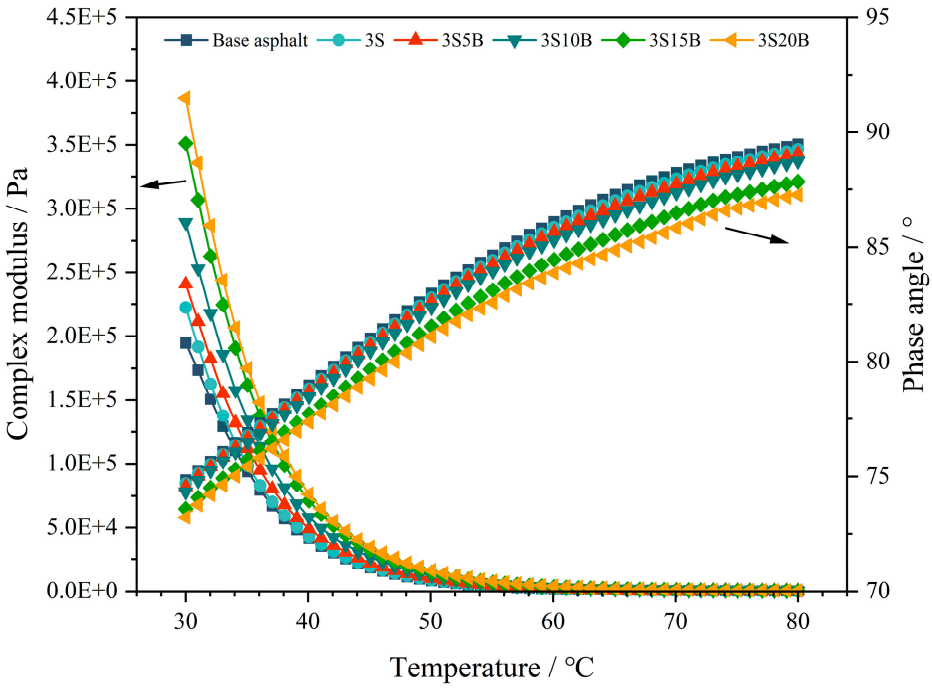


Figure 14. Temperature scan results at 30~80 °C.

The rutting factor is a parameter used to evaluate high-temperature anti-distortion, with larger values indicating stronger deformation resistance. Figure 15 demonstrates that when the temperature rises, the rutting factor for all of the samples drops noticeably. However, adding Sasobit raises the rutting factor of the raw asphalt, as confirmed by the findings of the rotational viscosity test. Additionally, the addition of BRA further improves the rutting factor due to the higher asphaltene content of the BRA modifier, which absorbs the lighter components of WMA and improving the rigidity of BCMWMA, thus enhancing the deformation resistance of the asphalt.

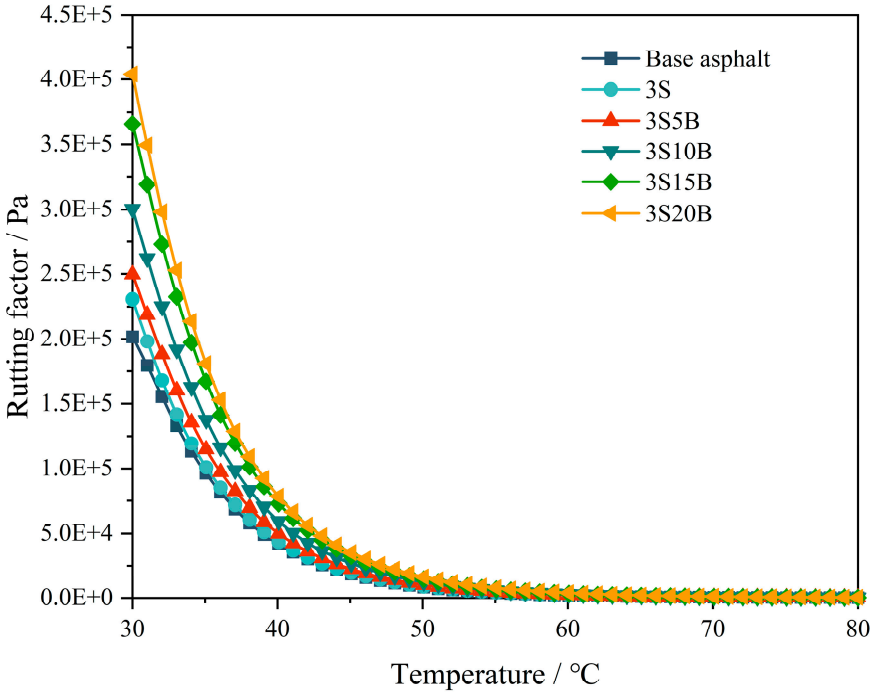


Figure 15. The result of the rutting factor (30~80 °C).

3.6. Frequency Sweep Test Results

Figures 16 and 17 show, respectively, the results of each test sample's G^* and δ at various temperatures. Figures reveal that the G^* of the same test specimen decreases with temperature increase, whereas the δ increases. Furthermore, the G^* of the test specimens increase with BRA doping at the same test temperature, while the δ shows the opposite trend. These observations are consistent with the temperature scan results. Additionally, the phase angle rises with frequency increase whereas the complex modulus decreases at the same test sample and the same temperature.

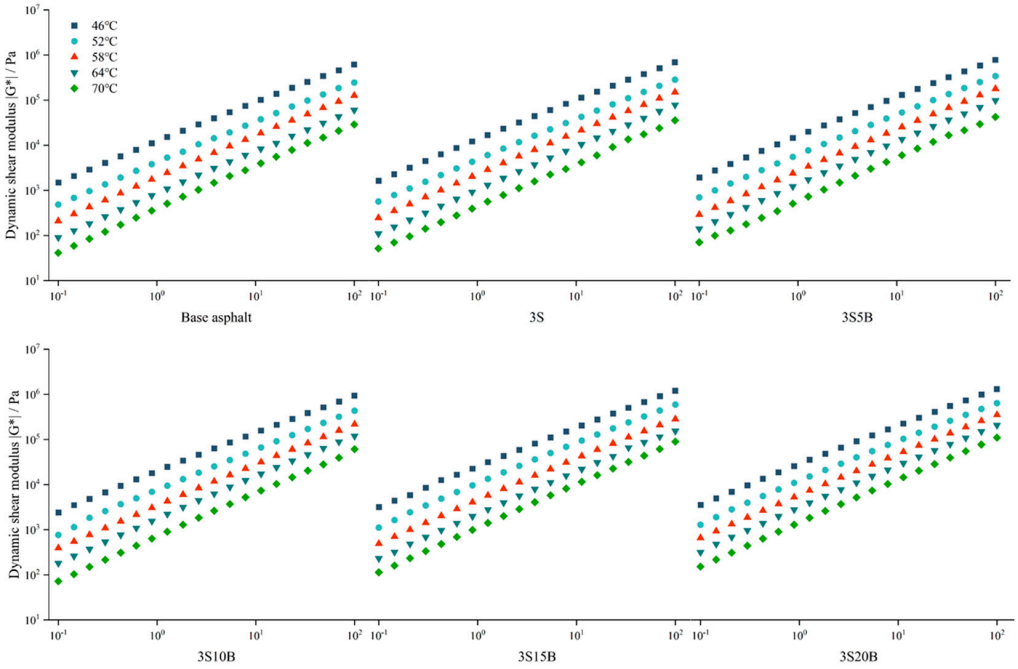


Figure 16. Results of complex modulus of frequency sweep test at different temperatures.

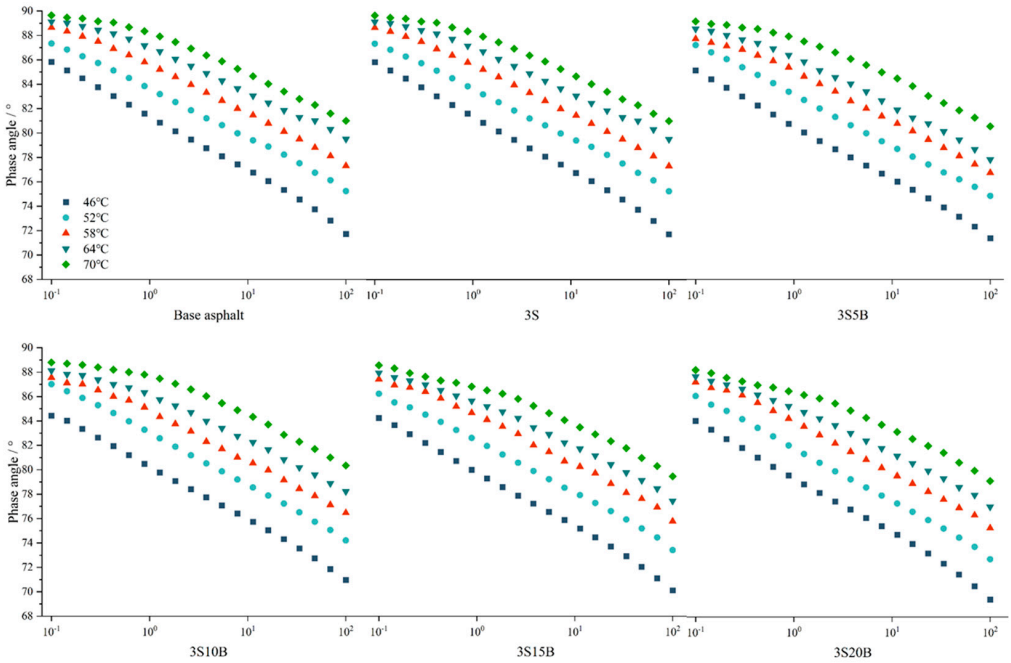


Figure 17. Results of phase angle of frequency sweep test at different temperatures.

3.7. MSCR Test Results

The strain evolution of asphalt samples was analyzed at various stress levels at 58 °C, and Figure 18 depicts the outcomes. The study found that the base asphalt accumulated the most strain, whereas with increasing BRA content, the accumulated strain of the BCMWMA has fallen steadily. Therefore, the use of BRA increased the WMA's rigidity and rutting resistance.

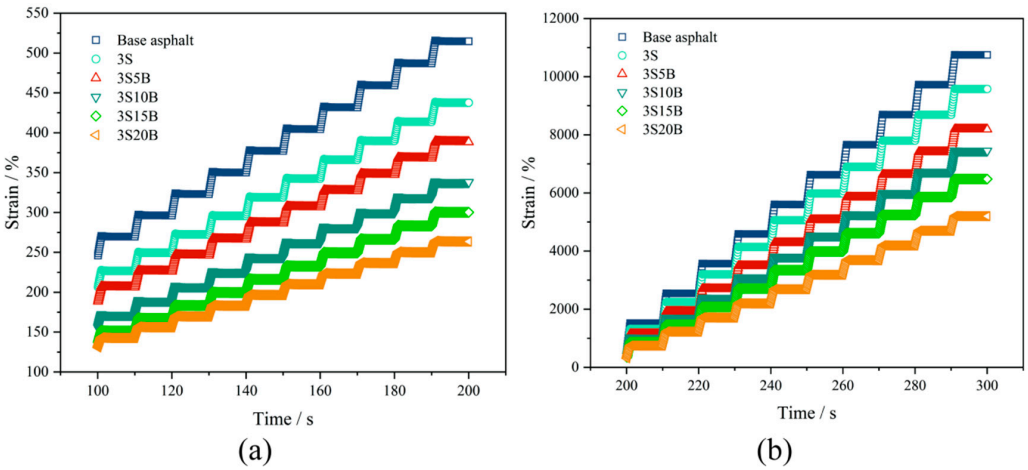


Figure 18. The creep and recovery curves of the asphalt samples at 58 °C: (**a**) 0.1 kPa, (**b**) 3.2 kPa.

To illustrate the creep recovery properties of test specimens, the parameters R, J_{nr} and $J_{nr-diff}$ are calculated. Generally, higher R and J_{nr} values indicate better creep recovery and poorer rutting resistance, respectively. While higher $J_{nr-diff}$ values suggest greater stress level effects on the amount of the J_{nr}.

The study found that the BRA positively affected the asphalt creep recovery rate at different load levels (0.1 kPa and 3.2 kPa), as depicted in Figures 19 and 20. The creep recovery rate of the specimens tested at both stress levels increased gradually as the BRA admixture increased, while the J_{nr} decreased. This shows that the BRA modifier enhanced WMA's resistance to rutting. Specifically, 3S20B showed a 133% increase in $R_{3.2}$ and a 38.8%

decrease in $J_{nr3.2}$ compared to 3S. The maximum value of $J_{nr-diff}$ of the samples tested in this study was 23.92% of that of the 3S sample, which is much less than the maximum allowable value of 75% of ASTM D7405-15 [62]. The warm agent improved the stress sensitivity of BCMWMA, and with the increase of BRA doping, the $J_{nr-diff}$ of the test sample gradually decreased. Moreover, 3S20B's $J_{nr-diff}$ showed the largest decreasing gradient, which was 28.93% lower than 3S15B and 35.91% lower than 3S samples. This indicates that the BRA reduced the stress sensitivity of WMA. This may be because the incorporation of BRA narrowed the gap of asphalt molecular chains, and at higher stress levels, external stresses acted more on the asphalt molecular chains, making it easier for WMA to produce recoverable deformation, which in turn improved the elastic properties of the tested samples. The improved elasticity and stiffness reduced the stress sensitivity of WMA. Meanwhile, the study also found that the BRA improved the viscosity and rigidity of asphalt, as shown by the findings of the temperature scan test. This enhancement ultimately made modified warm mix asphalt more resistant to rutting at high temperatures.

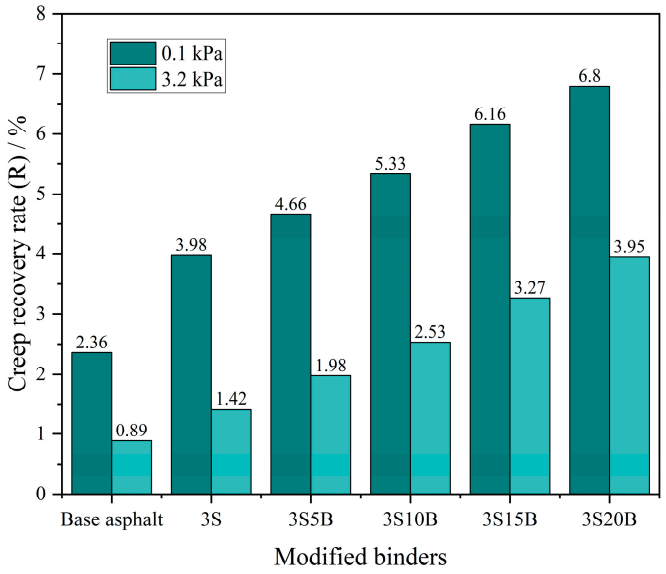


Figure 19. The results of creep recovery rate.

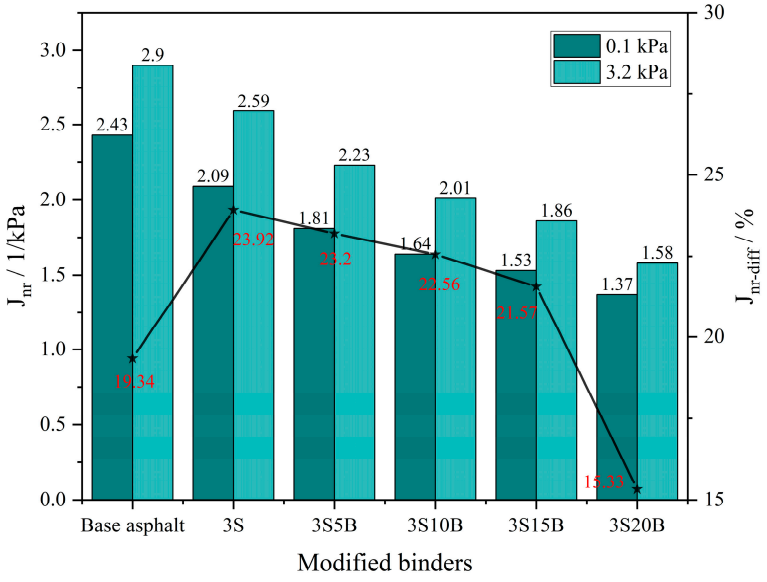


Figure 20. The results of the non-recoverable creep compliance and the percent difference of it.

Finally, the AASHTO M332 standard also states that the amount of traffic on the road should be taken into account when choosing an asphalt binder. Standard traffic load (S), high traffic load (H), extremely heavy traffic load (V), and extra-heavy traffic load (E) are the four categories for traffic levels. Table 9 displays traffic volume and J_{nr} − 3.2 kPa specifications. From Figure 20 and Table 9, it can be observed that the J_{nr} − 3.2 values of the base asphalt, 3S, 3S5B, and 3S10B are 2.9 kPa, 2.59 kPa, 2.23 kPa, and 2.01 kPa, respectively. These values are all below 4.5 kPa but greater than 2 kPa, indicating that they can withstand the standard traffic load. Furthermore, the J_{nr} − 3.2 values of 3S15B and 3S20B are 1.86 kPa and 1.58 kPa, respectively, which are below 2 kPa but greater than 1 kPa. This suggests that they are capable of withstanding the heavy traffic load of 58 °C.

Table 9. The traffic levels and J_{nr} − 3.2 kPa requirements.

Traffic Levels	S	H	V	E
J_{nr} − 3.2 kPa	≤4.5	≤2	≤1	≤0.5

4. Conclusions

Investigating the micromechanism and rheological characteristics of BRA and Sasobit composite modified asphalt was the goal of this research. To achieve this, several experiments were conducted. The physical and chemical properties, conventional properties, viscosity-temperature properties, rheological properties and storage stability of BCMWMA were investigated using SEM, FTIR, RV, DSR and BBR. Based on these experiments, the following conclusions were drawn:

(1) The FTIR spectral test results did not show any new characteristic peaks, indicating that the composite modification process involves physical co-mingling. The complex morphological characteristics of BRA particles are favorable for binding with asphalt, but the increase in BRA doping leads to enhanced ash agglomeration, which is unfavorable for the stability of the three-phase system in BCMWMA.

(2) BRA reduced the ductility and penetration of WMA while increasing the viscosity and softening point. Furthermore, it negatively affected the storage stability of BCMWMA. However, doping amounts below 15 wt% indicate the existence of a suitable dosing for a multi-phase equilibrium.

(3) BRA can enhance the high-temperature viscosity of WMA and increase the energy threshold required for to occur, while reducing the temperature sensitivity of WMA. BCMWMA, with BRA dosing at 15 wt% and below, exhibits a noticeable warm mixing effect.

(4) The higher the BRA doping, the poorer the low-temperature performance becomes. The maximum allowed doping of BRA to meet the specification is 15 wt%, with a low temperature threshold of −12 °C. BRA enhances the stiffness of WMA across a wide temperature range and frequency domain. BCMWMA meets the requirements for standard traffic and heavy traffic loading according to the AASHTO M332 standard.

Author Contributions: Conceptualization, W.L., Q.J. and Z.Z.; Methodology, W.L., Q.J., X.Y. and J.X.; Investigation, X.Y.; Writing—original draft, W.L.; Writing—review & editing, Z.Z. and J.X.; Supervision, S.W.; Project administration, S.W. All authors have read and agreed to the published version of the manuscript.

Funding: Hubei Science and Technology Innovation Talent and Service Project (International Science and Technology Cooperation) with grant number 2022EHB006, funded by the Key Research and Development Program of Hubei Province. Key R&D Program of Guangxi Province with grant number 2021AB26023.

Institutional Review Board Statement: Not applicable.

Informed Consent Statement: Not applicable.

Data Availability Statement: All data, models, and code generated or used during the study appear in the submitted article.

Acknowledgments: The authors wish to thank the State Key Laboratory of Silicate Materials for Architectures for providing experimental equipment. Meanwhile, thanks for Linjie Zhu from Keyango (www.sci-go.com, accessed on 15 October 2022) for the SEM analysis.

Conflicts of Interest: The authors declare no conflict of interest.

References

1. Bíl, M.; Vodák, R.; Kubeček, J.; Bílová, M.; Sedoník, J. Evaluating Road Network Damage Caused by Natural Disasters in the Czech Republic between 1997 and 2010. *Transp. Res. Part A Policy Pract.* **2015**, *80*, 90–103. [CrossRef]
2. Yadykova, A.Y.; Ilyin, S.O. Bitumen Improvement with Bio-Oil and Natural or Organomodified Montmorillonite: Structure, Rheology and Adhesion of Composite Asphalt Binders. *Constr. Build. Mater.* **2023**, *364*, 129919. [CrossRef]
3. Huang, T.; Cao, Z.; Lv, S.; Yu, H.; Peng, X.; Jiang, H.; Wu, L. Road Behavior and Micro Characteristics of High-Performance Asphalt Based on Compound Modification Approach. *Constr. Build. Mater.* **2023**, *371*, 130622. [CrossRef]
4. Sirin, O.; Paul, D.K.; Kassem, E. State of the Art Study on Aging of Asphalt Mixtures and Use of Antioxidant Additives. *Adv. Civ. Eng.* **2018**, *2018*, e3428961. [CrossRef]
5. Yang, B.; Li, H.; Sun, Y.; Zhang, H.; Liu, J.; Yang, J.; Zhang, X. Chemo-Rheological, Mechanical, Morphology Evolution and Environmental Impact of Aged Asphalt Binder Coupling Thermal Oxidation, Ultraviolet Radiation and Water. *J. Clean. Prod.* **2023**, *388*, 135866. [CrossRef]
6. Zhang, H.; Su, M.; Zhao, S.; Zhang, Y.; Zhang, Z. High and Low Temperature Properties of Nano-Particles/Polymer Modified Asphalt. *Constr. Build. Mater.* **2016**, *114*, 323–332. [CrossRef]
7. Xie, J.; Chen, J.; Hu, L.; Wu, S.; Wang, Z.; Li, M.; Yang, C. Preparation, Thermochromic Properties and Temperature Controlling Ability of Novel Pellets in Ultra-Thin Wearing Course. *Constr. Build. Mater.* **2023**, *389*, 131797. [CrossRef]
8. Li, J.; Yu, J.; Wu, S.; Xie, J. The Mechanical Resistance of Asphalt Mixture with Steel Slag to Deformation and Skid Degradation Based on Laboratory Accelerated Heavy Loading Test. *Materials* **2022**, *15*, 911. [CrossRef]
9. Wang, K.; Cheng, X.; Zhu, Y.; Li, H. Study on Performance Deterioration Regularity of Hot Regenerated Asphalt Mixture under Multiple Aging Factors. *Constr. Build. Mater.* **2023**, *369*, 130568. [CrossRef]
10. Yang, X.; Liu, G.; Zhang, H.; Meng, Y.; Peng, C.; He, X.; Liang, J. Aging Behavior of Polyphosphoric Acid/Styrene-Butadiene-Styrene-Modified Bio-Mixed Asphalt Based on High-Temperature Rheological Properties and Microscopic Mechanism. *Constr. Build. Mater.* **2023**, *389*, 131691. [CrossRef]
11. Wang, C.; Huang, S.; Chen, Q.; Ji, X.; Duan, K. Materials, Preparation, Performances and Mechanism of Polyurethane Modified Asphalt and Its Mixture: A Systematic Review. *J. Road Eng.* **2023**, *3*, 16–34. [CrossRef]
12. Zeng, G.; Shen, A.; Lyu, Z.; Kang, C.; Cui, H.; Ren, G.; Yue, G. Research on Anti-Aging Properties of POE/SBS Compound-Modified Asphalt in High-Altitude Regions. *Constr. Build. Mater.* **2023**, *376*, 131060. [CrossRef]
13. Han, Y.; Cui, B.; Tian, J.; Ding, J.; Ni, F.; Lu, D. Evaluating the Effects of Styrene-Butadiene Rubber (SBR) and Polyphosphoric Acid (PPA) on Asphalt Adhesion Performance. *Constr. Build. Mater.* **2022**, *321*, 126028. [CrossRef]
14. Nazari, H.; Naderi, K.; Moghadas Nejad, F. Improving Aging Resistance and Fatigue Performance of Asphalt Binders Using Inorganic Nanoparticles. *Constr. Build. Mater.* **2018**, *170*, 591–602. [CrossRef]
15. Wang, R.; Xu, G.; Chen, X.; Zhou, W.; Zhang, H. Evaluation of Aging Resistance for High-Performance Crumb Tire Rubber Compound Modified Asphalt. *Constr. Build. Mater.* **2019**, *218*, 497–505. [CrossRef]
16. Zhang, H.; Zhang, Y.; Chen, J.; Liu, W.; Wang, W. Effect of Desulfurization Process Variables on the Properties of Crumb Rubber Modified Asphalt. *Polymers* **2022**, *14*, 1365. [CrossRef]
17. Yang, C.; Wu, S.; Xie, J.; Amirkhanian, S.; Zhao, Z.; Xu, H.; Wang, F.; Zhang, L. Development of Blending Model for RAP and Virgin Asphalt in Recycled Asphalt Mixtures via a Micron-Fe_3O_4 Tracer. *J. Clean. Prod.* **2023**, *383*, 135407. [CrossRef]
18. Lu, W.; Peng, X.; Lv, S.; Yang, Y.; Wang, J.; Wang, Z.; Xie, N. High-Temperature Properties and Aging Resistance of Rock Asphalt Ash Modified Asphalt Based on Rutting Index. *Constr. Build. Mater.* **2023**, *363*, 129774. [CrossRef]
19. Zhao, P.; Song, X.; Dong, M.; Sun, H.; Wu, W.; Zhang, R.; Sun, M.; Zhao, X. Preparation and Characterization of CQDs/SBS Composites and Its Application Performance as Asphalt Modifier. *Constr. Build. Mater.* **2022**, *320*, 126312. [CrossRef]
20. Gong, X.; Liu, Q.; Wang, H.; Wan, P.; Chen, S.; Wu, J.; Wu, S. Synthesis of Environmental-Curable CO_2-Based Polyurethane and Its Enhancement on Properties of Asphalt Binder. *J. Clean. Prod.* **2023**, *384*, 135576. [CrossRef]
21. Lv, Y.; Wu, S.; Li, N.; Cui, P.; Wang, H.; Amirkhanian, S.; Zhao, Z. Performance and VOCs Emission Inhibition of Environmentally Friendly Rubber Modified Asphalt with UiO-66 MOFs. *J. Clean. Prod.* **2023**, *385*, 135633. [CrossRef]
22. Cai, L.; Shi, X.; Xue, J. Laboratory Evaluation of Composed Modified Asphalt Binder and Mixture Containing Nano-Silica/Rock Asphalt/SBS. *Constr. Build. Mater.* **2018**, *172*, 204–211. [CrossRef]
23. Huang, W.; Lv, Q.; Xiao, F. Investigation of Using Binder Bond Strength Test to Evaluate Adhesion and Self-Healing Properties of Modified Asphalt Binders. *Constr. Build. Mater.* **2016**, *113*, 49–56. [CrossRef]
24. Yan, K.; Li, Y.; Long, Z.; You, L.; Wang, M.; Zhang, M.; Diab, A. Mechanical Behaviors of Asphalt Mixtures Modified with European Rock Bitumen and Waste Cooking Oil. *Constr. Build. Mater.* **2022**, *319*, 125909. [CrossRef]

25. Anupam, K.; Akinmade, D.; Kasbergen, C.; Erkens, S.; Adebiyi, F. A State-of-the-Art Review of Natural Bitumen in Pavement: Underlining Challenges and the Way Forward. *J. Clean. Prod.* **2023**, *382*, 134957. [CrossRef]
26. Wang, M.; Xing, C. Evaluation of Microstructural Features of Buton Rock Asphalt Components and Rheological Properties of Pure Natural Asphalt Modified Asphalt. *Constr. Build. Mater.* **2021**, *267*, 121132. [CrossRef]
27. Lv, S.; Fan, X.; Yao, H.; You, L.; You, Z.; Fan, G. Analysis of Performance and Mechanism of Buton Rock Asphalt Modified Asphalt. *J. Appl. Polym. Sci.* **2019**, *136*, 46903. [CrossRef]
28. Lv, S.; Peng, X.; Liu, C.; Qu, F.; Zhu, X.; Tian, W.; Zheng, J. Aging Resistance Evaluation of Asphalt Modified by Buton-Rock Asphalt and Bio-Oil Based on the Rheological and Microscopic Characteristics. *J. Clean Prod.* **2020**, *257*, 120589. [CrossRef]
29. Lapian, F.E.P.; Ramli, M.I.; Pasra, M.; Arsyad, A. The Performance Modeling of Modified Asbuton and Polyethylene Terephthalate (PET) Mixture Using Response Surface Methodology (RSM). *Appl. Sci.* **2021**, *11*, 6144. [CrossRef]
30. Ren, J.; Xue, B.; Zhang, L.; Liu, W.; Li, D.; Xu, Y. Characterization and Prediction of Rutting Resistance of Rock Asphalt Mixture under the Coupling Effect of Water and High-Temperature. *Constr. Build. Mater.* **2020**, *254*, 119316. [CrossRef]
31. Chang, S.-C.; Liao, M.-C.; Shen, D.-H. Evaluation of Engineering Properties of Rock-Modified Asphalt Concrete. *J. Test. Eval.* **2021**, *49*, 839–853. [CrossRef]
32. Li, R.; Karki, P.; Hao, P. Fatigue and Self-Healing Characterization of Asphalt Composites Containing Rock Asphalts. *Constr. Build. Mater.* **2020**, *230*, 116835. [CrossRef]
33. Qian, J.; Wang, Q.; Wu, W.; Zhang, H. Fatigue Performance of Gussasphalt Concrete Made from Modified AH-70# Asphalt. *Mater. Des.* **2013**, *52*, 686–692. [CrossRef]
34. Li, T.; Guo, Z.; Liang, D.; Luo, S.; Zhang, Y.; Hong, B.; Lu, G.; Wang, D.; Oeser, M. Chemical and Physical Effects of Polyurethane-Precursor-Based Reactive Modifier on the Low-Temperature Performance of Bitumen. *Constr. Build. Mater.* **2022**, *328*, 127055. [CrossRef]
35. Cheraghian, G.; Cannone Falchetto, A.; You, Z.; Chen, S.; Kim, Y.S.; Westerhoff, J.; Moon, K.H.; Wistuba, M.P. Warm Mix Asphalt Technology: An up to Date Review. *J. Clean. Prod.* **2020**, *268*, 122128. [CrossRef]
36. Mazumder, M.; Sriraman, V.; Kim, H.H.; Lee, S.-J. Quantifying the Environmental Burdens of the Hot Mix Asphalt (HMA) Pavements and the Production of Warm Mix Asphalt (WMA). *Int. J. Pavement Res. Technol.* **2016**, *9*, 190–201. [CrossRef]
37. Thives, L.P.; Ghisi, E. Asphalt Mixtures Emission and Energy Consumption: A Review. *Renew. Sustain. Energy Rev.* **2017**, *72*, 473–484. [CrossRef]
38. Chen, B.; Dong, F.; Yu, X.; Ren, S.; Zheng, C. Chemo-Rheological Characterization of Aging Behaviors of Warm-Mix High-Viscosity Modified Asphalt. *J. Mater. Civ. Eng.* **2022**, *34*, 04022342. [CrossRef]
39. Liu, H.; Zhang, Z.; Li, N.; Li, H.; Wang, P. Effect of Organic Montmorillonite on Rheological Properties of Sasobit Warm-Mix Asphalt and Analysis of Its Ultraviolet Aging Behaviors. *J. Mater. Civ. Eng.* **2022**, *34*, 04022339. [CrossRef]
40. Xu, L.; Ni, H.; Zhang, Y.; Sun, D.; Zheng, Y.; Hu, M. Porous Asphalt Mixture Use Asphalt Rubber Binders: Preparation and Noise Reduction Evaluation. *J. Clean. Prod.* **2022**, *376*, 134119. [CrossRef]
41. Ramesh, A.; Venkat Ramayya, V.; Sandeep Reddy, G.; Vinayaka Ram, V. Investigations on Fracture Response of Warm Mix Asphalt Mixtures with Nano Glass Fibres and Partially Replaced RAP Material. *Constr. Build. Mater.* **2022**, *317*, 126121. [CrossRef]
42. Abdollahi, S.F.; Karimi, M.M.; Jahanbakhsh, H.; Tabatabaee, N. Cracking Performance of Rubberized RAP Mixtures with Sasobit. *Constr. Build. Mater.* **2022**, *319*, 126090. [CrossRef]
43. Luo, S.; Qian, Z.; Yang, X.; Wang, H. Design of Gussasphalt Mixtures Based on Performance of Gussasphalt Binders, Mastics and Mixtures. *Constr. Build. Mater.* **2017**, *156*, 131–141. [CrossRef]
44. Sobhi, S.; Yousefi, A.; Behnood, A. The Effects of Gilsonite and Sasobit on the Mechanical Properties and Durability of Asphalt Mixtures. *Constr. Build. Mater.* **2020**, *238*, 117676. [CrossRef]
45. Sobhi, S.; Hesami, S.; Poursoltani, M.; Ayar, P.; Mullapudi, R.S. Coupled Effects of Gilsonite and Sasobit on Binder Properties: Rheological and Chemical Analysis. *J. Mater. Civ. Eng.* **2022**, *34*, 04021470. [CrossRef]
46. Li, Y.; Chen, J.; Yan, J.; Guo, M. Influence of Buton Rock Asphalt on the Physical and Mechanical Properties of Asphalt Binder and Asphalt Mixture. *Adv. Mater. Sci. Eng.* **2018**, *2018*, 2107512. [CrossRef]
47. ASTM International. *D04 Committee Test Method for Penetration of Bituminous Materials*; ASTM International: West Conshohocken, PA, USA, 2006.
48. ASTM International. *D08 Committee Test Method for Softening Point of Bitumen (Ring-and-Ball Apparatus)*; ASTM International: West Conshohocken, PA, USA, 2014.
49. ASTM International. *D04 Committee Test Method for Ductility of Asphalt Materials*; ASTM International: West Conshohocken, PA, USA, 2018.
50. ASTM International. *D08 Committee Test Method for Viscosity Determination of Asphalt at Elevated Temperatures Using a Rotational Viscometer*; ASTM International: West Conshohocken, PA, USA, 2023.
51. ASTM International. *D04 Committee Practice for Determining the Separation Tendency of Polymer from Polymer Modified Asphalt*; ASTM International: West Conshohocken, PA, USA, 2020.
52. ASTM International. *D04 Committee Test Method for Multiple Stress Creep and Recovery (MSCR) of Asphalt Binder Using a Dynamic Shear Rheometer*; ASTM International: West Conshohocken, PA, USA, 2020.
53. ASTM International. *D6648: Standard Test Method for Determining the Flexural Creep Stiffness of Asphalt Binder Using the Bending Beam Rheometer (BBR)*; ASTM International: West Conshohocken, PA, USA, 2016.

54. Eltwati, A.; Putra Jaya, R.; Mohamed, A.; Jusli, E.; Al-Saffar, Z.; Hainin, M.R.; Enieb, M. Effect of Warm Mix Asphalt (WMA) Antistripping Agent on Performance of Waste Engine Oil-Rejuvenated Asphalt Binders and Mixtures. *Sustainability* **2023**, *15*, 3807. [CrossRef]
55. Su, Y.; Hu, X.; Wan, J.; Wu, S.; Zhang, Y.; Huang, X.; Liu, Z. Physical Properties and Storage Stability of Buton Rock Asphalt Modified Asphalt. *Materials* **2022**, *15*, 3592. [CrossRef]
56. Tembe, E.; Tamele, L.; Buonocore, G.; Madivate, C.; Muiambo, H. Rheological and Thermo-Oxidative Aging Properties of Asphalt Modified with a Combination of Sasobit and Linear Low-Density Polyethylene. *Sustainability* **2023**, *15*, 4460. [CrossRef]
57. Zhao, Z.; Wu, S.; Liu, Q.; Xie, J.; Yang, C.; Wang, F.; Wan, P. Recycling Waste Disposable Medical Masks in Improving the Performance of Asphalt and Asphalt Mixtures. *Constr. Build. Mater.* **2022**, *337*, 127621. [CrossRef]
58. ASTM International. *D04 Committee Standard Viscosity-Temperature Chart for Asphalts*; ASTM International: West Conshohocken, PA, USA, 2017.
59. Liu, H.; Zhang, Z.; Xie, J.; Gui, Z.; Li, N.; Xu, Y. Analysis of OMMT Strengthened UV Aging-Resistance of Sasobit/SBS Modified Asphalt: Its Preparation, Characterization and Mechanism. *J. Clean. Prod.* **2021**, *315*, 128139. [CrossRef]
60. Zheng, M.; Liu, Y.; Liu, X.; Zhang, W.; Wang, F.; Liu, S. Study on the Viscoelastic Behaviour of the Modified Asphalt Containing Multi-Walled Carbon Nanotubes (MWCNTs) and Crumb Rubber (CR). *Constr. Build. Mater.* **2021**, *311*, 125244. [CrossRef]
61. Modifier for Asphalt Mixture. Part 5: Natural Asphalt. (JT/T 860.5-2014.). Available online: https://std.samr.gov.cn/hb/search/stdHBDetailed?id=8B1827F23807BB19E05397BE0A0AB44A (accessed on 14 June 2023).
62. Liu, H.; Zeiada, W.; Al-Khateeb, G.G.; Shanableh, A.; Samarai, M. Use of the Multiple Stress Creep Recovery (MSCR) Test to Characterize the Rutting Potential of Asphalt Binders: A Literature Review. *Constr. Build. Mater.* **2021**, *269*, 121320. [CrossRef]

Disclaimer/Publisher's Note: The statements, opinions and data contained in all publications are solely those of the individual author(s) and contributor(s) and not of MDPI and/or the editor(s). MDPI and/or the editor(s) disclaim responsibility for any injury to people or property resulting from any ideas, methods, instructions or products referred to in the content.